

FAST discovery of a fast neutral hydrogen outflow

RENZHI SU,^{1,2,3,4} MINFENG GU,² S. J. CURRAN,⁵ ELIZABETH K. MAHONY,⁴ NINGYU TANG,⁶ JAMES R. ALLISON,⁷
DI LI,^{8,1,9} MING ZHU,^{8,10} J. N. H. S. ADITYA,^{11,12} HYEIN YOON,^{11,12} ZHENG ZHENG,⁸ AND ZHONGZU WU¹³

¹Research Center for Intelligent Computing Platforms, Zhejiang Laboratory, Hangzhou 311100, China

²Key Laboratory for Research in Galaxies and Cosmology, Shanghai Astronomical Observatory, Chinese Academy of Sciences, 80 Nandan Road, Shanghai 200030, China

³University of Chinese Academy of Sciences, 19A Yuquan Road, Beijing 100049, China

⁴ATNF, CSIRO Space and Astronomy, PO Box 76, Epping, NSW 1710, Australia

⁵School of Chemical and Physical Sciences, Victoria University of Wellington, PO Box 600, Wellington 6140, New Zealand

⁶Department of Physics, Anhui Normal University, Wuhu, Anhui 241002, People's Republic of China

⁷First Light Fusion Ltd., Unit 9/10 Oxford Pioneer Park, Mead Road, Yarnton, Kidlington OX5 1QU, UK

⁸National Astronomical Observatories, Chinese Academy of Sciences, 20A Datun Road, Beijing 100101, China

⁹NAOC-UKZN Computational Astrophysics Centre, University of KwaZulu-Natal, Durban 4000, South Africa

¹⁰CAS Key Laboratory of FAST, National Astronomical Observatories, Chinese Academy of Sciences, Beijing 100101, China

¹¹Sydney Institute for Astronomy, School of Physics A28, University of Sydney, NSW 2006, Australia

¹²ARC Centre of Excellence for All Sky Astrophysics in 3 Dimensions (ASTRO 3D)

¹³College of Physics, Guizhou University, 550025 Guiyang, PR China

ABSTRACT

In this letter, we report the discovery of a fast neutral hydrogen outflow in SDSS J145239.38+062738.0, a merging radio galaxy containing an optical type I active galactic nuclei (AGN). This discovery was made through observations conducted by the Five-hundred-meter Aperture Spherical radio Telescope (FAST) using redshifted 21-cm absorption. The outflow exhibits a blueshifted velocity likely up to $\sim -1000 \text{ km s}^{-1}$ with respect to the systemic velocity of the host galaxy with an absorption strength of $\sim -0.6 \text{ mJy beam}^{-1}$ corresponding to an optical depth of 0.002 at $v = -500 \text{ km s}^{-1}$. The mass outflow rate ranges between 2.8×10^{-2} and $3.6 \text{ M}_{\odot} \text{ yr}^{-1}$, implying an energy outflow rate ranging between 4.2×10^{39} and $9.7 \times 10^{40} \text{ erg s}^{-1}$, assuming $100 \text{ K} < T_s < 1000 \text{ K}$. Plausible drivers of the outflow include the star bursts, the AGN radiation, and the radio jet, the last of which is considered the most likely culprit according to the kinematics. By analysing the properties of the outflow, the AGN, and the jet, we find that if the HI outflow is driven by the AGN radiation, the AGN radiation seems not powerful enough to provide negative feedback whereas the radio jet shows the potential to provide negative feedback. Our observations contribute another example of a fast outflow detected in neutral hydrogen, as well as demonstrate the capability of FAST in detecting such outflows.

Keywords: Interstellar absorption (831) – Interstellar atoms (833) – Jets (870) – Radio lines (1358)

1. INTRODUCTION

1.1. Background

Redshifted HI 21-cm absorption provides us with unique insights into the neutral gas in and around galaxies throughout the Universe (e.g. Morganti et al.

2015; Allison et al. 2022). Depending on whether the absorbing neutral hydrogen gas is along the line-of-sight or within the host galaxy of the background radio continuum source, HI absorption is classified as intervening (e.g. Kanekar et al. 2009, 2014; Curran 2021; Gupta et al. 2021a; Mahony et al. 2022) or associated (e.g. Allison et al. 2012, 2014; Curran et al. 2016; Maccagni et al. 2017; Gupta et al. 2021b; Murthy et al. 2021; Su et al. 2022).

While intervening HI absorbers are good tracers of cold neutral gas reservoir for star formation

surenzhiz@zhejianglab.com

gumf@shao.ac.cn

(e.g. Curran 2017, 2019), associated HI absorbers have been frequently utilized to investigate the accretion and feedback processes in active galactic nuclei (AGN) (e.g. Morganti et al. 2013; Mahony et al. 2013; Maccagni et al. 2014; Aditya 2019; Su et al. 2023). Generally, symmetric HI absorption components with full width at half maximum (FWHM) from several tens to a few hundreds km s^{-1} centred on or close to the systemic velocity trace regularly rotating structures whereas asymmetric, broader, shallow, and blueshifted HI absorption components indicate the presence of outflows (e.g. Morganti et al. 2005; Curran et al. 2016). Outflows play an important role in galaxy evolution (e.g. Fabian 2012; Veilleux et al. 2020). However, currently direct detections of such HI outflows are quite rare, see the compilation by Morganti & Oosterloo (2018).

The detection of an outflow required a relatively large bandwidth in addition to sufficient sensitivity to detect low optical depths $\tau \sim 0.005$ (Morganti & Oosterloo 2018). If the background radio emission is weak (e.g. < 500 mJy), the detection becomes unfeasible over a reasonable observing time. The advent of the Five-hundred-meter Aperture Spherical radio Telescope (FAST; Nan et al. 2011, 2016; Li et al. 2018; Jiang et al. 2019, 2020) gives us an ideal tool to explore such shallow HI outflows by utilizing its large collecting area. Recent observations have demonstrated the FAST capability in detecting HI absorption lines (Zhang et al. 2021; Hu et al. 2023).

1.2. Optical and radio properties of SDSS J145239.38+062738.0

SDSS J145239.38+062738.0 (hereafter J1452+0627) is a merging galaxy at redshift $z = 0.26716$, which exhibits a tail (Ahumada et al. 2020), see its optical image in Figure 1 (Dey et al. 2019). It is a type I AGN showing broad (FWHM > 2000 km s^{-1}) $\text{H}\alpha$ emission, showing high ionisation lines and is located in Seyfert region of the BPT diagram (Baldwin, Philips, & Terlevich diagram; a tool used for classifying galaxies based on emission lines; Baldwin et al. 1981; Murthy et al. 2021). In the radio band, it has been classified as a flat-spectrum quasar (Healey et al. 2007; Souchay et al. 2012). The very long baseline interferometry (VLBI) images at C band (4.3 GHz) and X band (7.6 GHz) of J1452+2627 were obtained from the Astrogro VLBI image database¹ (Schinzel et al. 2017), as shown in Figure 2. We note that the images were produced (by the provider) like those presented in Petrov (2021). The C band image has

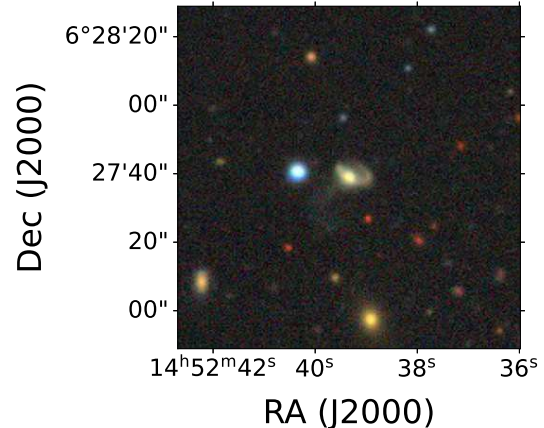


Figure 1. The *grz* composite image of J1452+0627 (the central object) from the DESI Legacy Imaging Surveys (Dey et al. 2019), showing compelling evidence of tidal features indicating that J1452+0627 is a merging system.

a resolution of $4.2 \text{ mas} \times 1.9 \text{ mas}$ and reveals extended emission consisting of several components with a total flux of 167 mJy. The X band image has a slightly higher resolution of $2.3 \text{ mas} \times 1.1 \text{ mas}$ and exhibits a similar morphology with a total flux of 66 mJy. Usually, under \sim mas resolution, the radio emission from starbursts is spatially resolved. Although there is \sim mas scale radio emission detected in some extreme starburst galaxies such as Mrk 273 (Carilli & Taylor 2000; Bondi et al. 2005) and Arp 220 (Batejat et al. 2011; Varenus et al. 2019), the morphologies are a clumpy of unresolved bean-like components that are distinct from the VLBI images of J1452+0627. More importantly, J1452+0627 is a galaxy with star formation rate of just $\sim 6 M_{\odot} \text{ yr}^{-1}$, see Section 4.2, which is an order of magnitude less than those in extreme starburst galaxies. Therefore, its VLBI detected radio emission definitely come from jet. Previous observations using the Karl G. Jansky Very Large Array (JVLA) detected broad HI absorption towards it with a peak optical depth of 0.21 (Murthy et al. 2021). However, the blue side (< -240 km s^{-1}) and the red side (> 400 km s^{-1}) of the HI spectrum is impacted by radio frequency interference (RFI).

In this letter, we report the detection of a fast atomic hydrogen outflow using the FAST, revealed as a shallow and blueshifted HI absorption wing that was not detected in the previous JVLA observation (Murthy et al. 2021).

2. OBSERVATION AND DATA REDUCTION

J1452+0627 was observed in September 2022 using the ON-OFF mode as part of a programme to find 18-cm OH absorption in a sample of radio galaxies. The observations utilized the FAST L-band 19-beam receiver

¹ http://astrogro.org/vlbi_images/

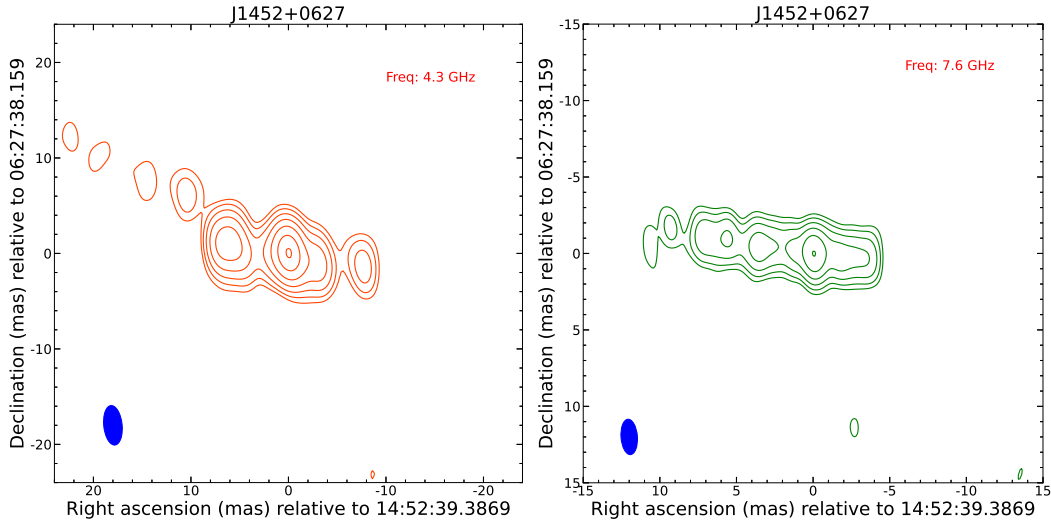


Figure 2. Left: the VLBI image of J1452+0627 at C band. The rms noise level is $0.2 \text{ mJy beam}^{-1}$ and the spatial resolution is $4.3 \text{ mas} \times 1.9 \text{ mas}$. The beam is shown in the lower-left corner. The contours are at 1.0, 2.0, 4.0, 8.0, 16.0, 32.0, 53.0 mJy beam^{-1} . Right: the VLBI image of J1452+0627 at X band. The rms noise level is $0.1 \text{ mJy beam}^{-1}$ and the spatial resolution is $2.4 \text{ mas} \times 1.1 \text{ mas}$. The beam is shown in the lower-left corner. The contours are at 0.5, 1.0, 2.0, 4.0, 8.0, 16.0 mJy beam^{-1} . Please note that both images were taken from the Astrogro VLBI image database.

covering 1.00–1.50 GHz over 65,536 channels. The large bandwidth also covered the redshifted HI 21-cm line. The ON and OFF times were set to 315 seconds and 15 ON-OFF cycles were used to observe the target. During the observation, all 19 beams, each with a field of view of ~ 3 arcmin (Jiang et al. 2020), were working simultaneously. Following Zheng et al. (2020), we selected a specific OFF point so that when the central beam 01 was off the source, beam 14 was on the source. Therefore, both beam 01 and 14 were observing J1452+0627 and the total on-source time is 9450 seconds. The data were recorded every 0.1 seconds and the high noise diode, $\sim 12.5 \text{ K}$, was injected for $5 \times 90 \text{ s}$ to calibrate the flux.

We reduced the XX and YY polarization data from beam 01 and 14 separately and then averaged them using Python-based codes written by ourselves. We first used the noise diode and the gain curves to calibrate the spectra flux. It is worth mentioning that the gain of beam 01 is different from that of beam 14, as reported in Jiang et al. (2020). Next, for each ON-OFF cycle, the OFF-target spectrum was subtracted from the ON-target spectrum to correct the bandpass. We used two methods to subtract the continuum.

Method 1: We implemented continuum subtraction individually for each polarization data and each ON-OFF cycle. A combination of a 3rd order polynomial and a sine functions was fitted to channels outside the range of 1119.3~1123.2 MHz to subtract the continuum. The fitting processes and results of beam 01 are shown in Figure 3, 4 while the beam 14 shows comparable results. Notably, the bandpass remained quite stable

throughout the observations and the XX and YY polarization data do not have much difference.

To quantify the stability of the bandpass within the range of 1118~1126 MHz, we take the XX polarization data of beam 01 as an example. First, we normalised the fitted continuums of the 15 ON-OFF cycles at 1122 MHz. Then we defined the variation of the bandpass for each ON-OFF cycle as $Vari_bp = \sqrt{\frac{\sum_{i=1}^n (\text{ContFit}_i - \text{ContAve}_i)^2}{n}}$, where ContFit_i represents the fitted continuum flux in the i th channel, ContAve_i is the averaged fitted continuum flux from all 15 ON-OFF cycles in the i th channel, and n is the total number of channels within the range of 1118~1126 MHz. Finally we obtained the average value $\overline{Vari_bp}$ for the 15 ON-OFF cycles of XX polarization data from beam 01, which is 0.0060. For YY polarization of beam 01, XX polarization of beam 14, and YY polarization of beam 14, the average value $\overline{Vari_bp}$ were found to be 0.0066, 0.0081 and 0.0058 respectively. It is worth noting that the $\overline{Vari_bp}$ for XX polarization of beam 14 is relatively higher, which is due to the relatively more pronounced standing waves in the first 5 ON-OFF cycles. If these cycles are excluded, the $\overline{Vari_bp}$ would decrease to 0.0047. Although the bandpass exhibits slight variation, we do not think it would affect our detection of absorption line. This is because the spectral continuums appear flat after continuum subtractions, indicating the continuum subtractions were good and thus the influence from bandpass has been removed, see Figure 3, 4.

Some RFI were identified which have been indicated by red arrows. We flagged these and averaged the 15 cycles data in each polarization. The results are shown in Figure 5. The XX and YY polarization data from both beam 01 and beam 14 exhibit obvious blueshifted wings, providing mutual confirmation of the existence of the wing.

Method 2: We first flagged all the RFI and averaged the 15 ON-OFF cycles data in each polarization. Then we used a combination of a 3rd order polynomial and a sine functions to fit channels outside the range of 1119.3~1123.2 MHz to subtract the continuums. The fitting processes and results are shown in Figure 6. The continuum subtractions were good as well. We did a comparison of the results between method 1 and method 2, which are presented in Figure 5. The results obtained from method 2 are remarkably similar to those acquired from method 1 except for that the red side continuum of spectra from beam 14 are flatter, indicating a bit better continuum subtractions.

Finally, the XX and YY polarization data from both beam 01 and beam 14 were averaged to generate a final spectrum. The final spectra through method 1 and method 2 were converted to the source rest frame and smoothed to 20 km s^{-1} using the Python-based code *SpectRes* (Carnall 2017), which are presented in Figure 7. The final spectra exhibit clear blueshifted wings and are consistent with each other. As the method 2 provides a bit better continuum subtraction to the red side spectra from beam 14, we will use the final spectrum through the method 2 as the spectrum of J1452+0627, which has an rms noise of $0.088 \text{ mJy beam}^{-1}$.

One key question is to where the blueshifted wing can extend. From Figure 7, it appears that the wing extends to around -1000 km s^{-1} . However, it is crucial to consider the the influence of data processing and spectral noise. As above, we think the continuum is well subtracted and the final spectrum is primarily affected by noise. To understand the impact of noise, we smoothed the spectra from -1000 km s^{-1} to v , where $-1000 \leq v \leq -200$, to one channel. The resulting channel would have a signal noise ratio (SNR) as a function of v , as illustrated in Figure 8. According to the SNR distribution, at $v = -840 \text{ km s}^{-1}$, the $\text{SNR} = 2.95 \simeq 3$. We thus argue that the wing between $v = -1000$ and -840 km s^{-1} may be influenced by noise whereas the wing in $v > -840 \text{ km s}^{-1}$ should be real.

In summary, we used two methods to do the continuum subtractions. Both methods yielded satisfactory results, providing consistent outcomes with a clear blueshifted wing, see Figure 7. The outflow likely extends to -1000 km s^{-1} . Throughout the paper, the -1000

km s^{-1} is adopted as the end point of the blueshifted wing in the calculations of its properties.

3. RESULTS

3.1. The FAST spectrum of J1452+0627

The reduced HI absorption spectrum of J1452+0627 is presented in Figure 7. A shallow and blueshifted wing is evident in the spectrum. The entire spectrum is broad, spanning from $\sim -1000 \text{ km s}^{-1}$ to $\sim 500 \text{ km s}^{-1}$. This profile aligns with the observations made by the JVLA (Murthy et al. 2021), as shown in the comparison depicted in Figure 9. However, our spectrum is less affected by RFI and has more than one order of magnitude higher sensitivity. Consequently our spectrum reveals a previously undetected shallow and blueshifted wing extending up to velocity of $\sim -1000 \text{ km s}^{-1}$.

We note that the detected absorption spectrum is a superposition of several Gaussian components arising from the absorbing gas. Since J1452+0627 is a merging galaxy, it suggests that the disk may be disturbed, thereby potentially increasing the velocity dispersion. Although the two deep absorption features in our spectrum may arise from disturbed disk gas, it is unlikely that this would lead to velocities up to $\sim -1000 \text{ km s}^{-1}$. It is worth noting that the optical image of J1452+0627 taken by the Hubble Space Telescope (HST) reveals a dust lane aligned along the radio emission (Murthy et al. 2021), implying that the radio jet is very likely expanding into a gas structure, thereby driving an outflow. Therefore, we propose that the observed blueshifted wing traces an outflow.

In our observation, we measured a continuum flux density of about $302 \pm 4 \text{ mJy beam}^{-1}$, where the error was determined from the uncertainty of the gain of FAST (Jiang et al. 2020), that is consistent with the JVLA observation which gave a peak flux density of $228.4 \text{ mJy beam}^{-1}$ and an integral flux density of 300.0 mJy .

In Murthy et al. (2021), the JVLA absorption spectrum was fitted with a disc model. However, the velocity dispersion fitted is quite high, $\sim 45 \text{ km s}^{-1}$ compared to a typical value of $\sim 10 \text{ km s}^{-1}$ (Struve et al. 2010), and the fitting would be worse if a lower velocity dispersion is used (Murthy et al. 2021), which is not surprising as the galaxy is a merging galaxy and thus any disk may have been disturbed or destroyed, indicating the HI spectrum cannot be interpreted with a regularly rotating disc model. Nevertheless, it is expected that most of the HI absorption arises from the disk, including the presence of the two deep absorption features.

To estimate the HI outflow properties, we adopted the blue wing part with $-1000 < v < -500 \text{ km s}^{-1}$ as a lower limit, and considered the entire blue side

Beam1 XX polarization fits

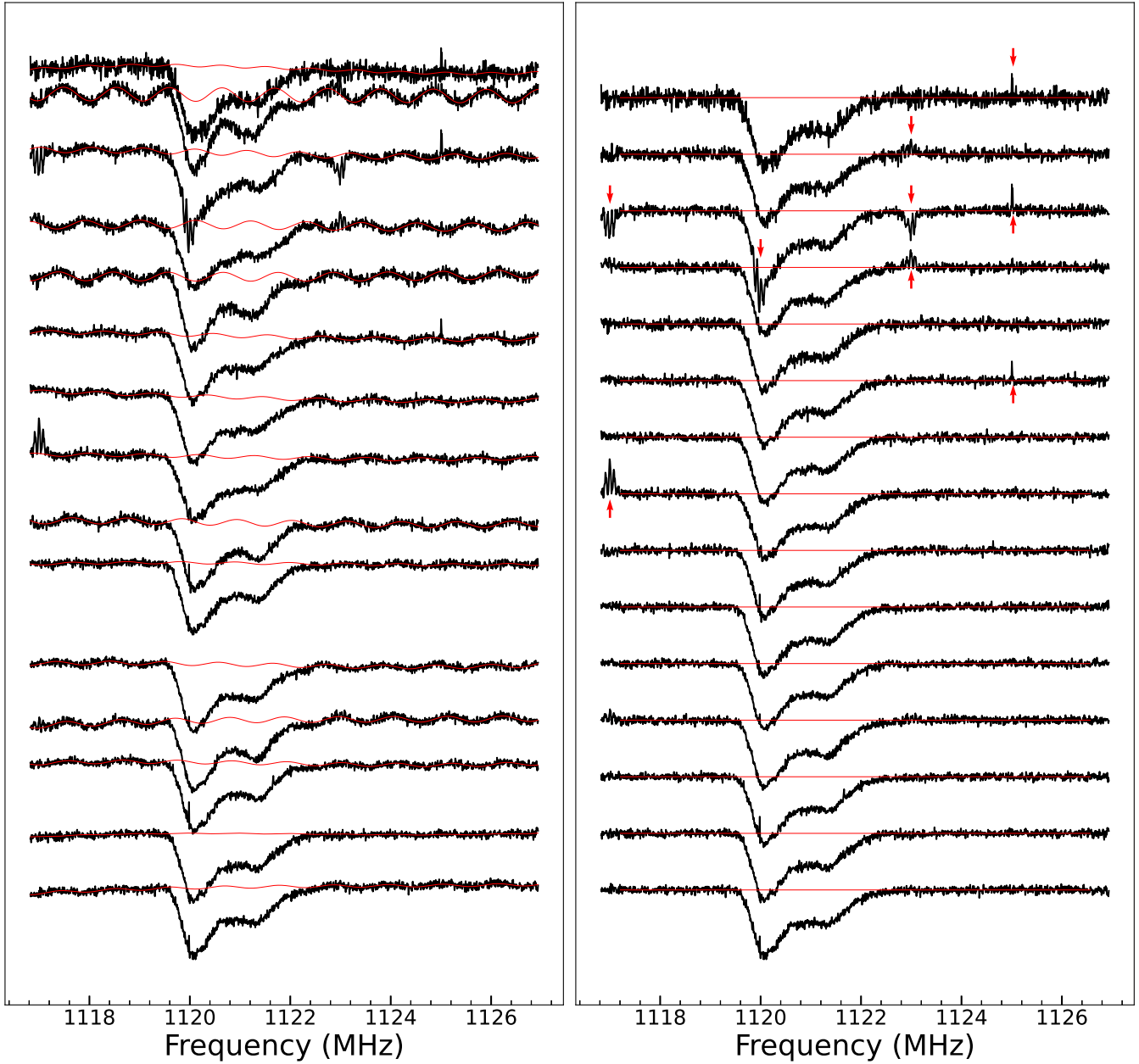


Figure 3. The continuum subtraction processes and results for XX polarization data of beam 1 using the method 1. Left: from top to bottom, the black lines are observed XX polarization spectra of beam 1 from ON-OFF cycle 1, 2, 3, 13, 14, 15. The red lines show the fitted continuum. The flux scale is normalised and spectra are offset for clarity. Right: the continuum-subtracted XX polarization spectra of beam 1 from ON-OFF cycle 1, 2, 3, 13, 14, 15. The red lines are horizontal. The flux scale is normalised and spectra are offset for clarity. Some RFI are indicated by red arrows. The spectral continua look flat after continuum subtractions, indicating the continuum subtractions were good.

Beam1 YY polarization fits

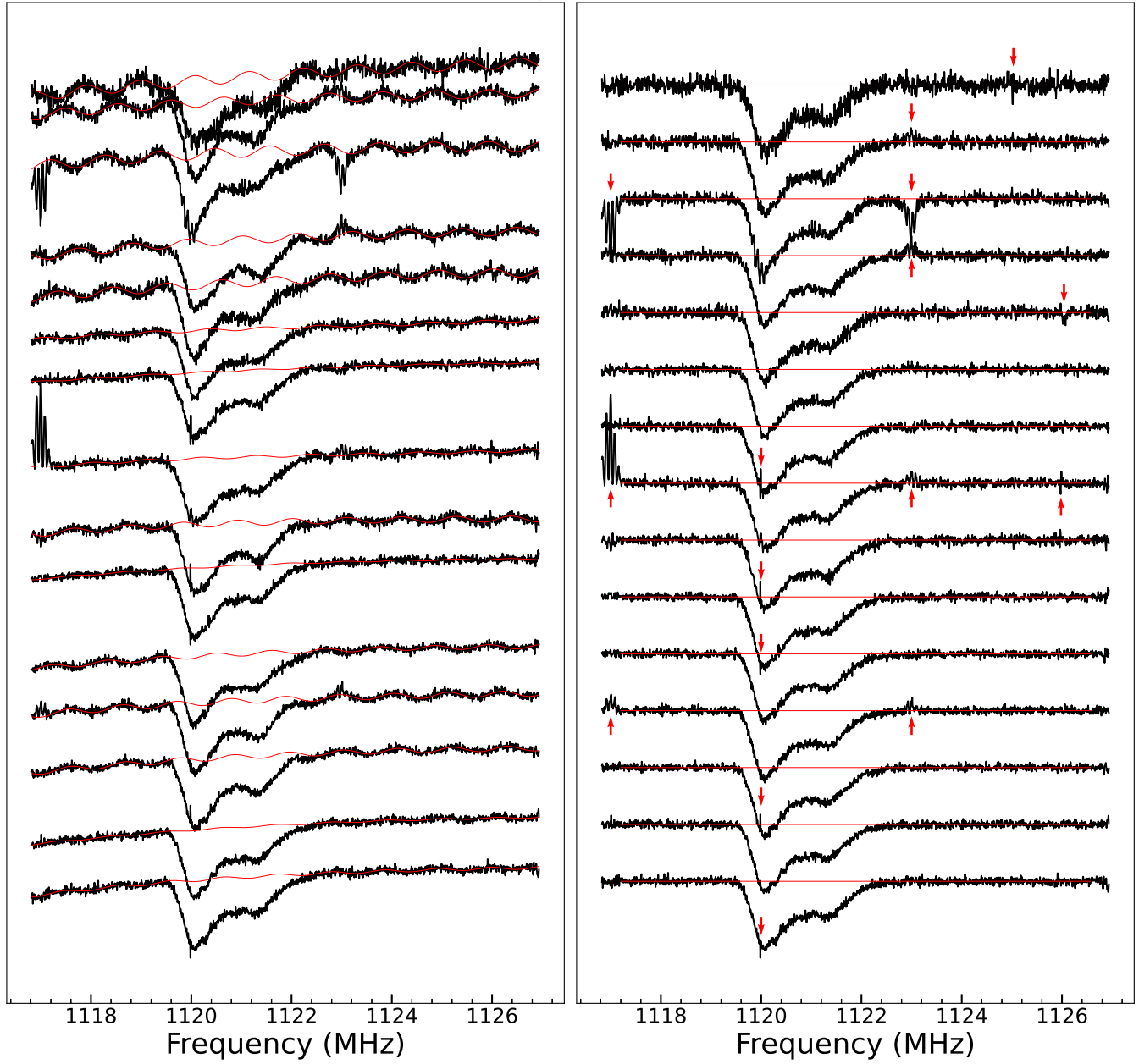


Figure 4. As Figure 3, but for YY polarization data of beam 1.

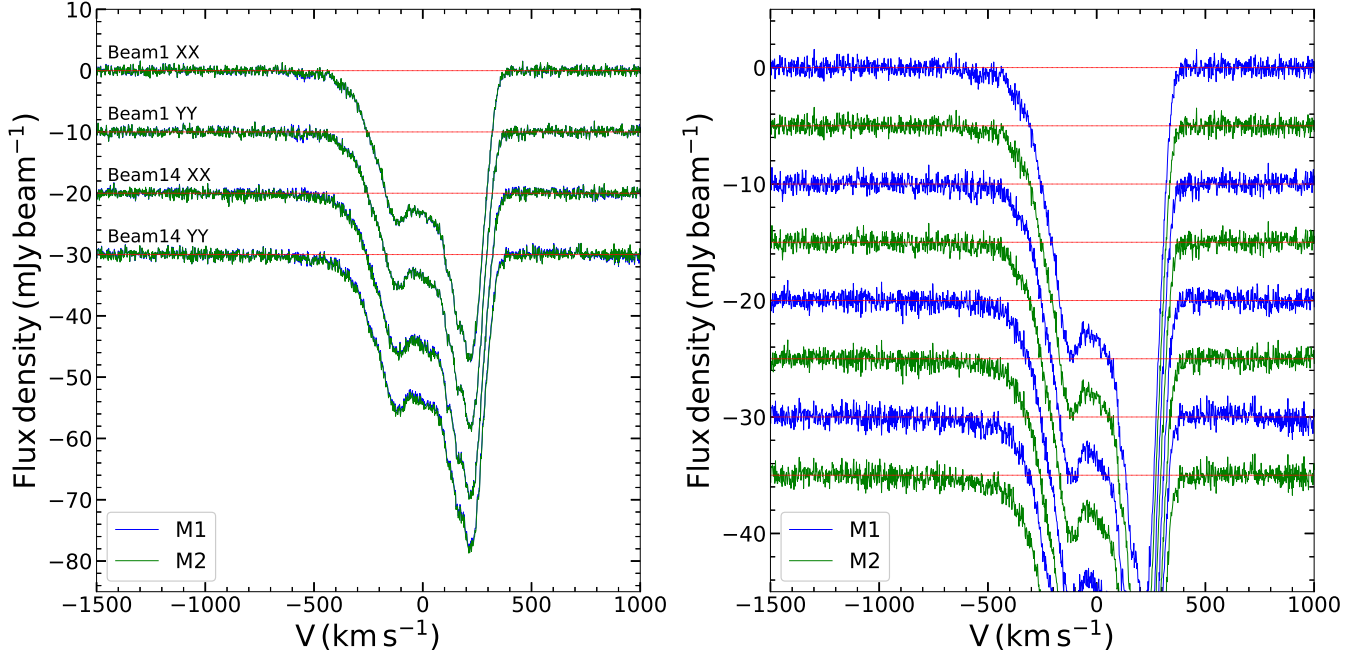


Figure 5. Left: the averaged and continuum subtracted spectra of beam 1 XX polarization, beam 1 YY polarization, beam 14 XX polarization, and beam 14 YY polarization. The beam 1 YY, beam 14 XX, and beam 14 YY are offset by -10, -20, and -30 respectively. The blue lines represent spectra produced through the method 1 while the green lines are those produced through the method 2. Right: the zoom-in plot of left but the spectra from the method 2 are more offset by -5 for a clear comparison. The method 2 gives a bit better continuum subtraction to the red side spectra from beam 14.

$v < 0 \text{ km s}^{-1}$ as an upper limit. Please note that these limits are reasonable. The absorption within the range of -1000 km s^{-1} to -500 km s^{-1} only represents a small fraction of the overall absorption, as depicted in Figure 7. The absorption strength at $v = -500 \text{ km s}^{-1}$ is approximately $\sim -0.6 \text{ mJy beam}^{-1}$, corresponding to an optical depth of 0.002. This feature was not detected in the JVLA observation and seems cannot be accounted for in the disc model fitting (Murthy et al. 2021). Thus, it is reasonable to consider this small portion as a lower limit. Additionally, taking the entire blue side ($v < 0 \text{ km s}^{-1}$) as an upper limit is also justified, as it likely contains a significant amount of absorption originating from the disc.

In HI absorption studies, the spin temperature T_s plays a crucial role in determining the HI column density. Usually, a fiducial value of 100 K (e.g. Aditya & Kanekar 2018a; Sadler et al. 2020) is often adopted when there is no direct measurement available for it. In the case of J1452+0627, considering that the VLBI images have scales of several tens of parsecs, it is reasonable to assume that the absorbing HI gas is located close to the central AGN. In such a scenario, a spin temperature of 1000 K seems plausible. Therefore, for the subsequent calculations, we will consider a range of $100 \text{ K} < T_s < 1000 \text{ K}$.

3.2. Outflow parameters

To estimate the mass and energy outflow rate, we use the formulae below (Heckman 2002):

$$dN_{\text{HI}} = 1.82 \times 10^{18} T_s \times \tau(v) dv \quad (1)$$

$$d\dot{M} = 30 \frac{\Omega}{4\pi} \frac{r_*}{1 \text{ kpc}} \frac{dN_{\text{HI}}}{10^{21} \text{ cm}^{-2}} \frac{v}{300 \text{ km s}^{-1}} M_{\odot} \text{ yr}^{-1} \quad (2)$$

$$\dot{M} = \int d\dot{M} \quad (3)$$

$$\dot{E} = \int \frac{1}{2} d\dot{M} v^2, \quad (4)$$

where T_s is spin temperature, τ is optical depth and equals to $-\ln[1 + \Delta S / (C_f S_{\text{cont}})]$ where ΔS is absorbed flux, C_f is covering factor, and S_{cont} is continuum flux, N_{HI} is HI column density, Ω is solid angle of outflow, r_* is radius of outflow, v is velocity of outflow, \dot{M} is mass outflow rate, and \dot{E} is energy outflow rate. While we can directly measure some parameters, we have to assume some other parameters. We assumed the covering factor is unit, which is an upper limit and often adopted when there is no direct measure it (e.g. Aditya & Kanekar 2018a,b; Su et al. 2022). We further assumed the Ω is π that is often used (e.g.

Beam1,14 XX YY polarization fits

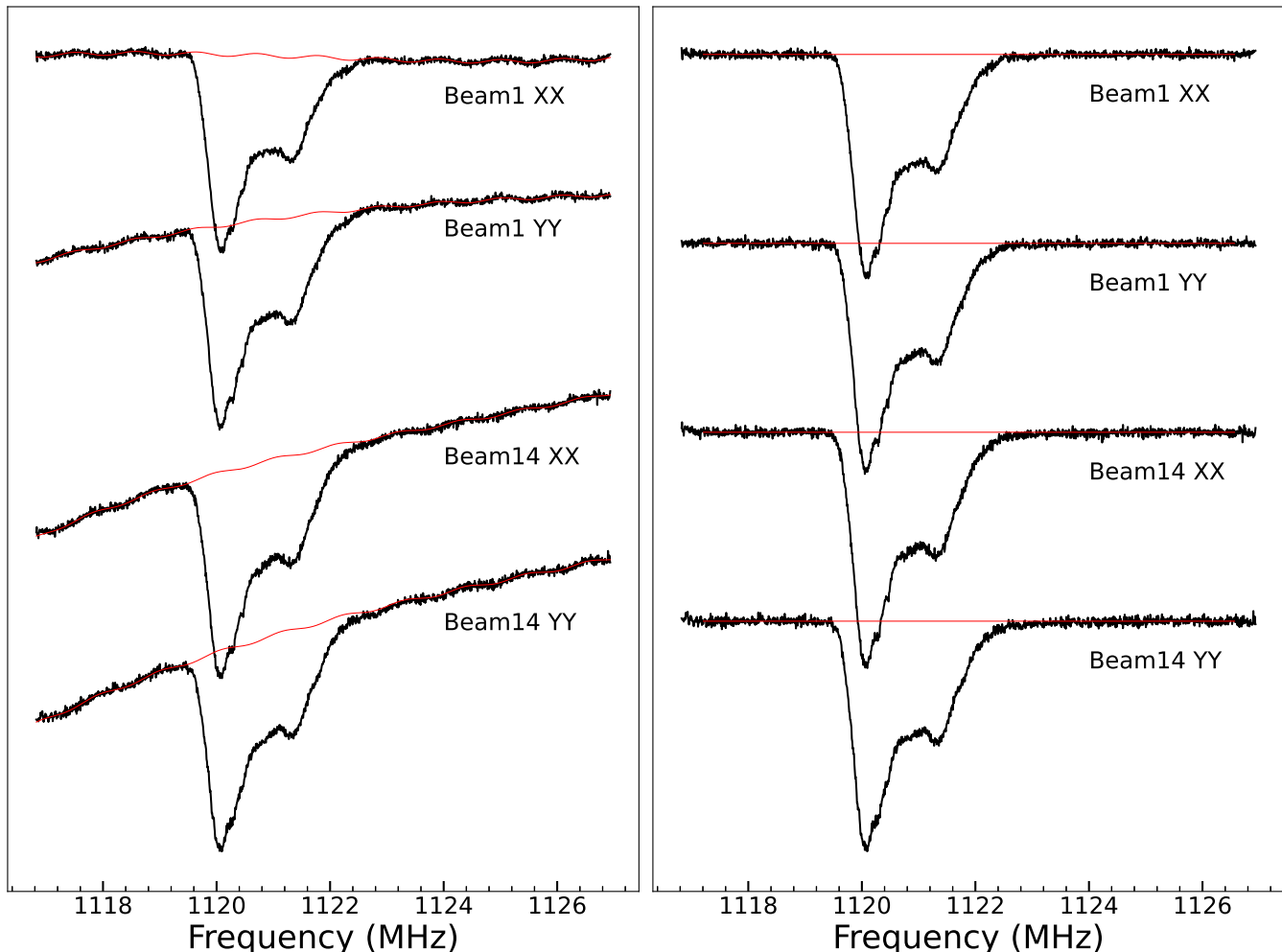


Figure 6. The continuum subtraction processes and results for XX and YY polarization data of beam 1 and 14 using the method 2. Left: from top to bottom, the black lines are spectra of beam 1 XX polarization, beam 1 YY polarization, beam 14 XX polarization, and beam 14 YY polarization, averaged from 15 ON-OFF cycles after flagging RFI. The red lines are fitted continuum. The y-axis is normalised and each next cycle spectrum is offset for clarity. Right: the black lines are corresponding continuum subtracted spectra of beam 1 XX polarization, beam 1 YY polarization, beam 14 XX polarization, and beam 14 YY polarization. The red lines are horizontal. The y-axis is normalised and each next cycle spectrum is offset for clarity. The flat continuums after continuum subtractions indicate the continuum subtractions were good as well.

Morganti et al. 2005; Aditya & Kanekar 2018b) and the r_* is half of the projected size of VLBI X-band emission (Murthy et al. 2021), ~ 25 pc. We also considered the velocity turbulence as this would give more accurate estimates, like the case of 3C 293 (e.g. Mahony et al. 2013). Finally, by integrating from -1000 km s^{-1} to -500 km s^{-1} and to 0 km s^{-1} and using $100 \text{ K} < T_s < 1000 \text{ K}$, we obtained a minimum mass outflow rate of $2.8 \times 10^{-2} M_{\odot} \text{ yr}^{-1}$ and a maximum mass outflow rate of $3.6 M_{\odot} \text{ yr}^{-1}$, corresponding to a minimum energy outflow rate of $4.2 \times 10^{39} \text{ erg s}^{-1}$ and a maximum energy outflow rate of $9.7 \times 10^{40} \text{ erg s}^{-1}$. We have summarized the outflow properties in Table 1.

4. DISCUSSION

4.1. Previous observations of J1452+0627

J1452+0627 was detected in HI absorption in JVLA observations and showed a full width at zero intensity (FWZI) $\sim 800 \text{ km s}^{-1}$ (Murthy et al. 2021). Besides, it has been also observed by the SDSS. We fitted the SDSS spectrum of J1452+0627 with PyQSOFit (Guo et al. 2018) that can simultaneously correct the Galaxy extinction, fit spectra with galaxy and AGN components, fit emission lines with Gaussian functions and drive emission line properties. Some key fitting results are summarized in Table 1. The [O III] $\lambda 5007$

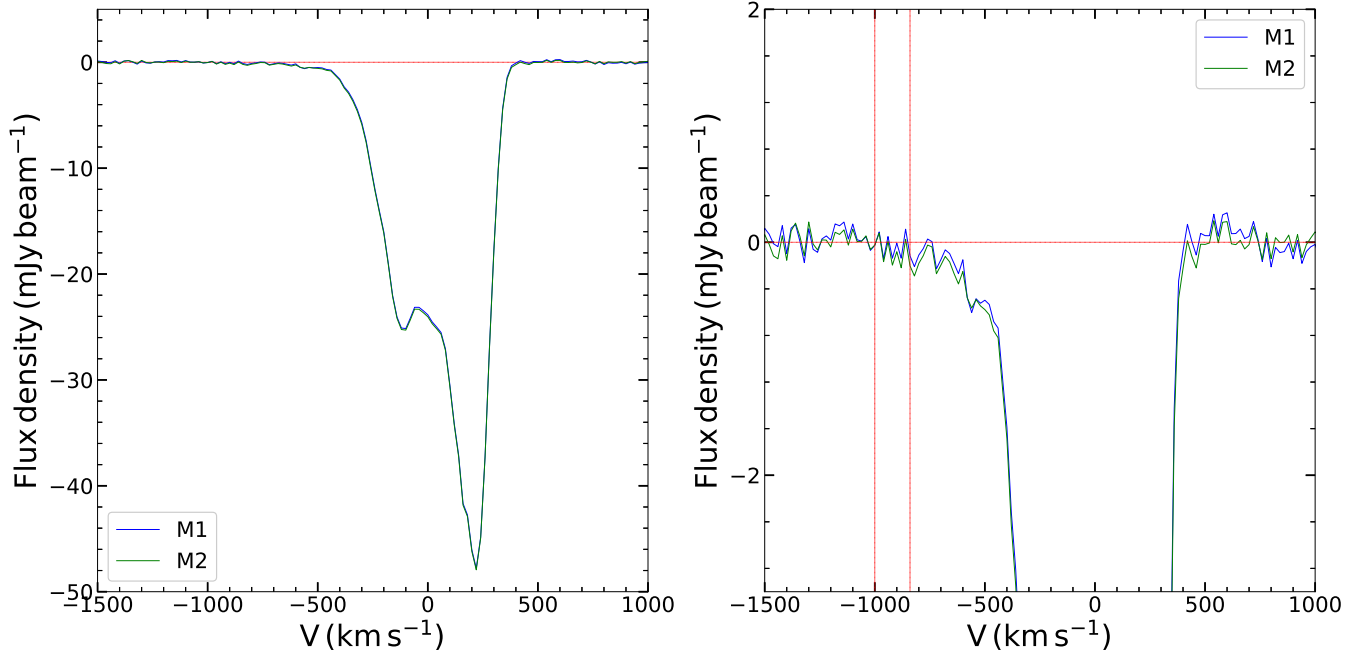


Figure 7. Left: the HI absorption spectra of J1452+0627 that shows a shallow and blueshifted wing, indicating an outflow. The blue line represents the one produced from the method 1 and the green line the one from the method 2. Both spectra are highly consistent with each other. Right: the zoom-in spectrum to more clearly show the shallow wing. The spectra have a velocity resolution of 20 km s^{-1} . As the method 2 can give a bit better continuum subtraction to the red side spectra from beam 14, we will use the final spectrum through the method 2 as the spectrum of J1452+0627, which has an rms noise of $0.088 \text{ mJy beam}^{-1}$. The two red vertical lines mark velocities at $v = -1000$ and -840 km s^{-1} . If smoothing this velocity range to one channel, the channel would have 2.95σ significance.

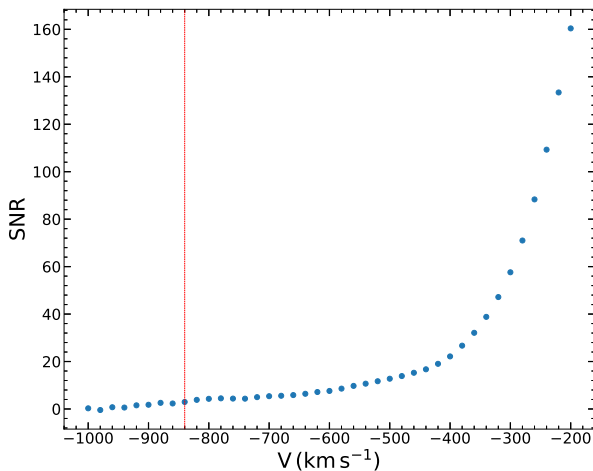


Figure 8. The SNR of the channel that smoothed from -1000 km s^{-1} to v , where $-1000 \leq v \leq -200 \text{ km s}^{-1}$. The vertical line marks $v = -840 \text{ km s}^{-1}$ at where the $\text{SNR} = 2.95 \simeq 3$. We thus argue that the wing between $v = -1000$ and -840 km s^{-1} may be influenced by noise whereas the wing in $v > -840 \text{ km s}^{-1}$ should be real.

line is best fitted with two components of which one has a FWHM 690 km s^{-1} while the another has a FWHM 1454 km s^{-1} and blueshifted by 254 km s^{-1} , which is con-

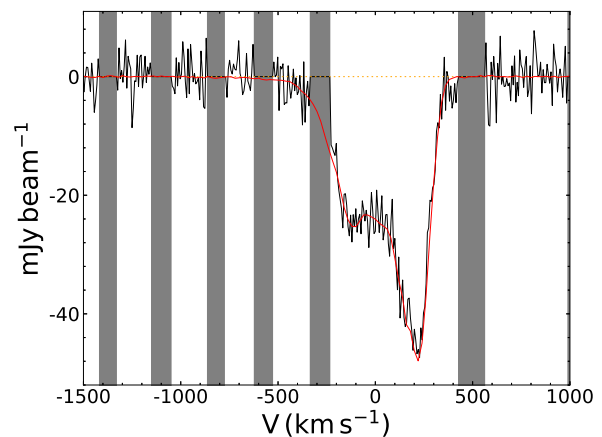


Figure 9. Comparison between our FAST spectrum (red line) and the JVLA spectrum (black line), showing consistent line parameters. The grey regions mark the channels affected by RFI in the JVLA spectrum.

sistent with the fitting results in [Murthy et al. \(2021\)](#). In the JVLA observations where the HI absorption width is close to that of the narrow [O III] $\lambda 5007$ component, [Murthy et al. \(2021\)](#) suggested these two phases of the gas might be associated. Our FAST observation that has much lower rms noise revealed that the HI line

Table 1. The properties of J1452+0627

J1452+0627	
Mass outflow rate:	$2.8 \times 10^{-2} - 3.6 M_{\odot} \text{ yr}^{-1}$
Energy outflow rate:	$4.2 \times 10^{39} - 9.7 \times 10^{40} \text{ erg s}^{-1}$
Jet power:	$\sim 5.8 \times 10^{43} \text{ erg s}^{-1}$
SMBH mass:	$\sim 1.6 \times 10^8 M_{\odot}$
Broad H α luminosity:	$\sim 1.1 \times 10^{42} \text{ erg s}^{-1}$
AGN bolometric luminosity:	$\sim 2.4 \times 10^{44} \text{ erg s}^{-1}$
Broad [O III] $\lambda 5007$ luminosity:	$\sim 5.5 \times 10^{41} \text{ erg s}^{-1}$
Broad [O III] $\lambda 5007$ FWHM:	1454 km s^{-1}
Narrow [O III] $\lambda 5007$ luminosity:	$\sim 8.5 \times 10^{41} \text{ erg s}^{-1}$
Narrow [O III] $\lambda 5007$ FWHM:	690 km s^{-1}
[N II] $\lambda 6584$ luminosity:	$\sim 8.3 \times 10^{41} \text{ erg s}^{-1}$
[O II] $\lambda 3727$ luminosity:	$\sim 2.9 \times 10^{41} \text{ erg s}^{-1}$
Star formation rate:	$\sim 6 M_{\odot} \text{ yr}^{-1}$

could be as broad as $\sim 1500 \text{ km s}^{-1}$ (FWZI) with a shallow component blueshifted up to $\sim -1000 \text{ km s}^{-1}$, suggesting that we maybe detected the neutral counterpart of the broad and blueshifted optical kinematic component. We have overlaid the HI absorption profile on the [O III] $\lambda 5007$ line profile in Figure 10.

4.2. Driving mechanism

A key question is what drives the outflow. Both starburst and AGN can produce outflows (e.g. Di Matteo et al. 2005; Veilleux et al. 2005; Booth & Schaye 2009; Morganti & Oosterloo 2018; Veilleux et al. 2020). In the case of J1452+0627, which is identified as an AGN, estimating the star formation rate through the commonly used H α line is not applicable. However, an alternative method based on the recalibration of the [O II] $\lambda 3727$ emission line can be employed to estimate the star formation rate in AGN (Zhuang & Ho 2019). By fitting the SDSS spectrum of J1452+0627, we obtained its [N II] $\lambda 6584$, [O II] $\lambda 3727$ and narrow [O III] $\lambda 5007$ emission lines luminosity and then derived a star formation rate of $\sim 6 M_{\odot} \text{ yr}^{-1}$ using the Equation 7 in Zhuang & Ho (2019).

The mass outflow rate that can be driven by this star formation rate was estimated as $\sim 1.5 M_{\odot} \text{ yr}^{-1}$ following Equation 1 in Veilleux et al. (2005), which is larger than or consistent with the observed mass outflow rate in J1452+0627, indicating that the star formation is able to drive the observed outflow.

The AGN could be the reasonable power source of the HI outflow. We estimated the AGN bolometric luminosity using $L_{\text{bol}} \simeq 30L_{\text{BLR}}$ (Xu et al. 2009), where L_{BLR} is

the luminosity of broad-line region and can be estimated from broad H α line (Celotti et al. 1997). By fitting the spectrum, we found the H α line can be fitted with a broad component (FWHM $> 2000 \text{ km s}^{-1}$). The broad component has a luminosity of $\sim 1.1 \times 10^{42} \text{ erg s}^{-1}$ which gives a bolometric luminosity of $\sim 2.4 \times 10^{44} \text{ erg s}^{-1}$.

Therefore, the ratio between energy outflow rate and AGN bolometric luminosity is between 1.7×10^{-5} and 4.0×10^{-4} which is much smaller than those in AGN energy-conserving wind-driven outflows (e.g. King 2010; Zubovas & King 2012; Costa et al. 2014) and those required to produce the $M - \sigma$ relation and powerful feedback (e.g. Di Matteo et al. 2005; Booth & Schaye 2009; Hopkins & Elvis 2010), indicating the AGN radiation has enough power to drive the HI outflow.

Simulations and observations suggest that radio jets can drive powerful outflows when they expand through the ISM of the host galaxy (e.g. Wagner & Bicknell 2011; Wagner et al. 2012; Mahony et al. 2013; Morganti et al. 2013). A radio jet could drive gas to high velocity if the ratio of jet power to Eddington luminosity $\eta = P_{\text{jet}}/L_{\text{Edd}}$ is above 10^{-4} (e.g. Wagner & Bicknell 2011; Wagner et al. 2012). To estimate the jet power, it is necessary to determine the radio emission contribution from star formation first. Given a star formation rate of $\sim 6 M_{\odot} \text{ yr}^{-1}$, the Equation 3 in Sullivan et al. (2001) provides an estimate of the maximum luminosity of $5.3 \times 10^{28} \text{ erg s}^{-1} \text{ Hz}^{-1}$ at 1.4 GHz. However, with FAST observations, a continuum flux density of $302 \pm 4 \text{ mJy}$ at 1.4 GHz was obtained, corresponding a luminosity of $6.7 \times 10^{32} \text{ erg s}^{-1} \text{ Hz}^{-1}$. This indicates the radio contribution from star formation is negligible. By using the Equation 2 in Best et al. (2006), the jet power is estimated to be $P_{\text{jet}} \sim 5.8 \times 10^{43} \text{ erg s}^{-1}$.

The SMBH mass can be estimated from the $M - \sigma$ relation (McConnell & Ma 2013). We used the Penalized PiXel-Fitting (pPXF) method (Cappellari & Emsellem 2004; Cappellari 2017, 2022) to fit the SDSS spectrum and obtained a stellar velocity dispersion $190 \pm 25.6 \text{ km s}^{-1}$ which gives a SMBH mass $\sim 1.6 \times 10^8 M_{\odot}$. Therefore, the η in J1452+0627 is $\sim 2.8 \times 10^{-3}$, meaning the radio jet is able to drive the observed HI outflow.

In summary, it seems the star formation, the AGN radiation, and the jet all can alone drive the observed HI outflow. Here we try to have a deeper analysis based on the HI outflow kinematics. The HI spectrum has a velocity likely blueshifted up to $\sim 1000 \text{ km s}^{-1}$ and a broad velocity width with a FWZI possibly up to $\sim 1500 \text{ km s}^{-1}$. Optical Na I D absorption line is a good indicator of HI gas. Previous Na I D absorption line observations have revealed that the HI outflows produced by large starbursts have an average FWHM of

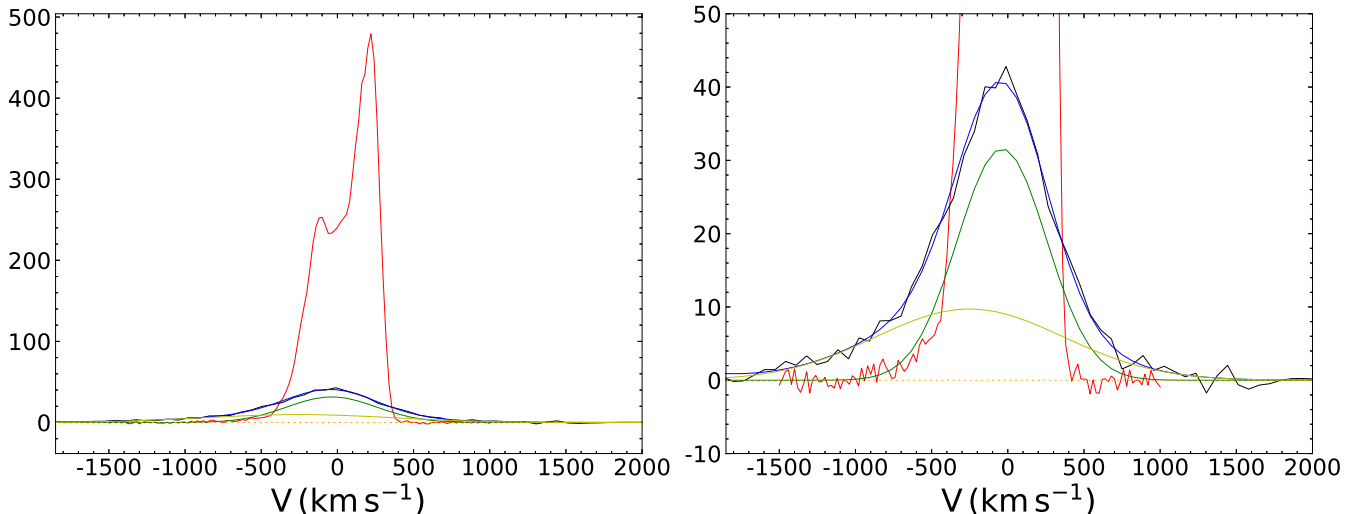


Figure 10. Left: The inverted FAST HI absorption line overlaid on the [O III] $\lambda 5007$ line. The y-axis is normalised. The red line is the inverted FAST HI absorption line. The black line is the [O III] $\lambda 5007$ line. The blue line is fitted [O III] $\lambda 5007$ line. The green line is fitted narrow [O III] $\lambda 5007$ component. The yellow line is fitted broad [O III] $\lambda 5007$ component. Right: the zoom-in of the left to make a clearer comparison.

$\sim 275 \text{ km s}^{-1}$ and an average maximum outflow velocity $\sim 300\text{--}400 \text{ km s}^{-1}$ (Veilleux et al. 2005). In comparison, it is very unlikely that the HI outflow in J1452+0627 is driven by starbursts. Broad Na I D absorption lines, typically $>500\text{--}600 \text{ km s}^{-1}$, have been detected before, but in jet-driven outflows (Lehnert et al. 2011). AGN radiation-driven outflows can have ionized gas with FWHM \sim a few thousands km s^{-1} and blueshifted by up to a few ten thousands km s^{-1} , like those in broad absorption line (BAL) quasars (Weymann et al. 1991; Gibson et al. 2009). However, it is not clear if the neutral gas in radiation-driven outflows can have similar kinematics or resemble that in our detected HI outflow. As of now, there is no observations to support this. In contrast, the kinematics of the HI outflow in J1452+0627 resemble those in jet-gas interactions (e.g. Morganti et al. 2005; Lehnert et al. 2011). For example, the jet-driven HI outflow in 4C 12.50 has a FWZI of $\sim 1600 \text{ km s}^{-1}$ and a maximum outflow velocity of $\sim 1200 \text{ km s}^{-1}$ (Morganti et al. 2005, 2013). Similarly, in 3C 293, the jet-driven HI outflow has a FWZI of $\sim 1400 \text{ km s}^{-1}$, of which $\sim 1000 \text{ km s}^{-1}$ are blueshifted (Mahony et al. 2013). More cases of jet-driven HI outflows that have similar kinematics can be seen in Morganti et al. (2005); Morganti & Oosterloo (2018). Therefore, based on the similar kinematics to know jet-driven outflows, the radio jet has the relatively higher probability, compared to the AGN radiation and star burst, to be the driver of the HI outflow in J1452+0627. But, we suggest that VLBI spectral line observations can help us locate the position of the

outflowing gas and thus pin down whether it is the radio jet that drives the outflow as the cases studied in, for example, 4C 12.50 (Morganti et al. 2013) and 3C 293 (Mahony et al. 2013).

4.3. Impact on the host galaxy

Based on whether the star formation is enhanced or suppressed, AGN-driven feedback is classified as ‘positive’ or ‘negative’. In this section, we will discuss whether the power source of the HI outflow in J1452+0627 can enhance or suppress star formation in the host galaxy. In hydrodynamical simulations setting ~ 5 per cent of AGN radiation can be injected to surrounding gas, it was found that the feedback would be powerful enough to quench star formation (Di Matteo et al. 2005). However, in a ‘two-phase’ model, an order of magnitude less injecting energy, ~ 0.5 per cent of AGN radiation, is capable of driving outflows to destroy cold gas reservoir and/or clear the gas out of the galaxy (Hopkins & Elvis 2010). The ratio between the energy outflow rate and the AGN bolometric luminosity in J1452+0627 is between 1.7×10^{-5} and 4.0×10^{-4} . Therefore, if the HI outflow is driven by AGN radiation, the AGN radiation seems not powerful enough to provide negative feedback.

As discussed in the last section, it is more likely the HI outflow is driven by the radio jet which has a power of $\sim 5.8 \times 10^{43} \text{ erg s}^{-1}$. In hydrodynamical simulations that have pc scale spatial resolution to study the interactions between jets and ISM (Wagner & Bicknell 2011; Wagner et al. 2012), it was found that the jet-induced feedback is effective enough to disperse cloudy gas and

thus inhibit star formation if jets have power in the range of 10^{43} – 10^{46} erg s $^{-1}$ and jets power to Eddington luminosity $\eta = P_{\text{jet}}/L_{\text{Edd}}$ is above 10^{-4} . In J1452+0627, the $P_{\text{jet}} \sim 5.8 \times 10^{43}$ erg s $^{-1}$ and the $\eta \sim 2.8 \times 10^{-3}$, therefore the jet seems have the potential to provide negative feedback.

In summary, if the HI outflow is driven by the AGN radiation, the AGN radiation seems not powerful enough to provide negative feedback whereas the radio jet seems have the potential to provide negative feedback.

5. CONCLUSION

In this paper, we report the discovery of a fast neutral outflow in J1452+0627 with the FAST. The outflow exhibits a blueshifted wing extending up to -1000 km s $^{-1}$. The absorption strength of the outflow at -500 km s $^{-1}$ is approximately -0.6 mJy beam $^{-1}$, corresponding to an optical depth of 0.002. The weak absorption strength and low optical depth indicate that detecting such outflows is very challenging because it is hard to go down to such low optical depth towards most radio sources within reasonable on-source times by using most current radio telescopes. The FAST telescope with its large collecting area is a fantastic tool to detect such faint outflows as demonstrated by our observations. Our discovery represents the first detection of a fast outflow by the FAST. It is expected more such detections will be made with the FAST telescope. So far, the detections of fast, broad, and shallow neutral outflows are rare, see the compilation by [Morganti & Oosterloo \(2018\)](#).

The main results associated with the outflow are summarized below:

- The outflow exhibits a mass outflow rate ranging from $2.8 \times 10^{-2} M_{\odot} \text{ yr}^{-1}$ to $3.6 M_{\odot} \text{ yr}^{-1}$, corresponding to an energy outflow rate between 4.2×10^{39} erg s $^{-1}$ and 9.7×10^{40} erg s $^{-1}$, assuming $100 \text{ K} < T_s < 1000 \text{ K}$.
- It seems the outflow is more likely driven by the jet based on the kinematics, although the starbursts and the AGN radiation cannot be ruled out as power sources. To elucidate the driving mechanism of the outflow and more accurately estimate the impact on the host galaxy, VLBI spectral observations are needed to localise the outflow.
- The ratio between energy outflow rate and AGN bolometric luminosity was found to be between 1.7×10^{-5} and 4.0×10^{-4} , which is smaller than that required to strikingly impact gas reservoir and thus suppress star formation ([Hopkins & Elvis 2010](#)), indicating that if the HI outflow is driven by the AGN radiation, the AGN radiation seems not powerful enough to provide negative feedback.
- The jet in J1452+0627 seems have the potential to provide negative feedback because the jet has a power

of $P_{\text{jet}} \sim 5.8 \times 10^{43}$ erg s $^{-1}$ and the ratio between jet power and Eddington luminosity is 2.8×10^{-3} which meet the criteria to inhibit star formation in simulations ([Wagner & Bicknell 2011](#); [Wagner et al. 2012](#)).

ACKNOWLEDGMENTS

We thank the anonymous referee for the constructive comments which have greatly improved the draft.

We thank the staff of the FAST who have made these observations possible. We thank Suma Murthy who provided the JVLA spectrum of J1452+0627 and Hengxiao Guo who fitted the SDSS spectrum of J1452+0627 with the pPXF.

This work made use of the data from FAST (Five-hundred-meter Aperture Spherical radio Telescope). FAST is a Chinese national mega-science facility, operated by National Astronomical Observatories, Chinese Academy of Sciences.

This work made use of the Astrogro VLBI FITS image database.

The Legacy Surveys consist of three individual and complementary projects: the Dark Energy Camera Legacy Survey (DECaLS; Proposal ID #2014B-0404; PIs: David Schlegel and Arjun Dey), the Beijing-Arizona Sky Survey (BASS; NOAO Prop. ID #2015A-0801; PIs: Zhou Xu and Xiaohui Fan), and the Mayall z-band Legacy Survey (MzLS; Prop. ID #2016A-0453; PI: Arjun Dey). DECaLS, BASS and MzLS together include data obtained, respectively, at the Blanco telescope, Cerro Tololo Inter-American Observatory, NSF’s NOIRLab; the Bok telescope, Steward Observatory, University of Arizona; and the Mayall telescope, Kitt Peak National Observatory, NOIRLab. Pipeline processing and analyses of the data were supported by NOIRLab and the Lawrence Berkeley National Laboratory (LBNL). The Legacy Surveys project is honored to be permitted to conduct astronomical research on Iolkam Du’ag (Kitt Peak), a mountain with particular significance to the Tohono O’odham Nation.

NOIRLab is operated by the Association of Universities for Research in Astronomy (AURA) under a cooperative agreement with the National Science Foundation. LBNL is managed by the Regents of the University of California under contract to the U.S. Department of Energy.

This project used data obtained with the Dark Energy Camera (DECam), which was constructed by the Dark Energy Survey (DES) collaboration. Funding for the DES Projects has been provided by the U.S. Department of Energy, the U.S. National Science Foundation, the Ministry of Science and Education of Spain,

the Science and Technology Facilities Council of the United Kingdom, the Higher Education Funding Council for England, the National Center for Supercomputing Applications at the University of Illinois at Urbana-Champaign, the Kavli Institute of Cosmological Physics at the University of Chicago, Center for Cosmology and Astro-Particle Physics at the Ohio State University, the Mitchell Institute for Fundamental Physics and Astronomy at Texas A&M University, Financiadora de Estudos e Projetos, Fundacao Carlos Chagas Filho de Amparo, Financiadora de Estudos e Projetos, Fundacao Carlos Chagas Filho de Amparo a Pesquisa do Estado do Rio de Janeiro, Conselho Nacional de Desenvolvimento Cientifico e Tecnologico and the Ministerio da Ciencia, Tecnologia e Inovacao, the Deutsche Forschungsgemeinschaft and the Collaborating Institutions in the Dark Energy Survey. The Collaborating Institutions are Argonne National Laboratory, the University of California at Santa Cruz, the University of Cambridge, Centro de Investigaciones Energeticas, Medioambientales y Tecnologicas-Madrid, the University of Chicago, University College London, the DES-Brazil Consortium, the University of Edinburgh, the Eidgenossische Technische Hochschule (ETH) Zurich, Fermi National Accelerator Laboratory, the University of Illinois at Urbana-Champaign, the Institut de Ciencies de l’Espai (IEEC/CSIC), the Institut de Fisica d’Altes Energies, Lawrence Berkeley National Laboratory, the Ludwig Maximilians Universitat Munchen and the associated Excellence Cluster Universe, the University of Michigan, NSF’s NOIRLab, the University of Nottingham, the Ohio State University, the University of Pennsylvania, the University of Portsmouth, SLAC National Accelerator Laboratory, Stanford University, the University of Sussex, and Texas A&M University.

BASS is a key project of the Telescope Access Program (TAP), which has been funded by the National Astronomical Observatories of China, the Chinese Academy of Sciences (the Strategic Priority Research Program “The Emergence of Cosmological Structures” Grant # XDB09000000), and the Special Fund for Astronomy from the Ministry of Finance. The BASS is also supported by the External Cooperation Program of Chinese Academy of Sciences (Grant # 114A11KYSB20160057), and Chinese National Natural Science Foundation (Grant # 12120101003, # 11433005).

The Legacy Survey team makes use of data products from the Near-Earth Object Wide-field Infrared Survey Explorer (NEOWISE), which is a project of the Jet Propulsion Laboratory/California Institute of Technology. NEOWISE is funded by the National Aeronautics and Space Administration.

The Legacy Surveys imaging of the DESI footprint is supported by the Director, Office of Science, Office of High Energy Physics of the U.S. Department of Energy under Contract No. DE-AC02-05CH1123, by the National Energy Research Scientific Computing Center, a DOE Office of Science User Facility under the same contract; and by the U.S. National Science Foundation, Division of Astronomical Sciences under Contract No. AST-0950945 to NOAO.

RZS is supported by NSFC grant No. 11988101, the National Science Foundation of China (grant 11873073), Shanghai Pilot Program for Basic Research-Chinese Academy of Science, Shanghai Branch (JCYJ-SHFY-2021-013), the National SKA Program of China (Grant No. 2022SKA0120102), the science research grants from the China Manned Space Project with NO. CMSCSST-2021-A06, and the Original Innovation Program of the Chinese Academy of Sciences (E085021002).

MFG is supported by the National Science Foundation of China (grant 11873073), Shanghai Pilot Program for Basic Research-Chinese Academy of Science, Shanghai Branch (JCYJ-SHFY-2021-013), the National SKA Program of China (Grant No. 2022SKA0120102), the science research grants from the China Manned Space Project with NO. CMSCSST-2021-A06, and the Original Innovation Program of the Chinese Academy of Sciences (E085021002).

DL is supported by NSFC grant No. 11988101.

ZZ is supported by NSFC grant No. 11988101, 12041302, and U1931110. ZZ is also supported by the science research grant from the China Manned Space Project with grant no. CMS-CSST-2021-A08.

N.-Y. Tang is sponsored by Zhejiang Lab Open Research Project (NO. K2022PE0AB01), Cultivation Project for FAST Scientific Payoff and Research Achievement of CAMS-CAS, National key R&D program of China under grant No. 2018YFE0202900 and the University Annual Scientific Research Plan of Anhui Province (NO.2022AH010013).

REFERENCES

Aditya, J. N. H. S. 2019, *MNRAS*, 482, 5597,

doi: [10.1093/mnras/sty3062](https://doi.org/10.1093/mnras/sty3062)

Aditya, J. N. H. S., & Kanekar, N. 2018a, *MNRAS*, 481,

1578, doi: [10.1093/mnras/sty2184](https://doi.org/10.1093/mnras/sty2184)

- . 2018b, *MNRAS*, 473, 59, doi: [10.1093/mnras/stx2325](https://doi.org/10.1093/mnras/stx2325)
- Ahumada, R., Allende Prieto, C., Almeida, A., et al. 2020, *ApJS*, 249, 3, doi: [10.3847/1538-4365/ab929e](https://doi.org/10.3847/1538-4365/ab929e)
- Allison, J. R., Sadler, E. M., & Meekin, A. M. 2014, *MNRAS*, 440, 696, doi: [10.1093/mnras/stu289](https://doi.org/10.1093/mnras/stu289)
- Allison, J. R., Curran, S. J., Emonts, B. H. C., et al. 2012, *MNRAS*, 423, 2601, doi: [10.1111/j.1365-2966.2012.21062.x](https://doi.org/10.1111/j.1365-2966.2012.21062.x)
- Allison, J. R., Sadler, E. M., Amaral, A. D., et al. 2022, *PASA*, 39, e010, doi: [10.1017/pasa.2022.3](https://doi.org/10.1017/pasa.2022.3)
- Baldwin, J. A., Phillips, M. M., & Terlevich, R. 1981, *PASP*, 93, 5, doi: [10.1086/130766](https://doi.org/10.1086/130766)
- Batejat, F., Conway, J. E., Hurley, R., et al. 2011, *ApJ*, 740, 95, doi: [10.1088/0004-637X/740/2/95](https://doi.org/10.1088/0004-637X/740/2/95)
- Best, P. N., Kaiser, C. R., Heckman, T. M., & Kauffmann, G. 2006, *MNRAS*, 368, L67, doi: [10.1111/j.1745-3933.2006.00159.x](https://doi.org/10.1111/j.1745-3933.2006.00159.x)
- Bondi, M., Pérez-Torres, M. A., Dallacasa, D., & Muxlow, T. W. B. 2005, *MNRAS*, 361, 748, doi: [10.1111/j.1365-2966.2005.09206.x](https://doi.org/10.1111/j.1365-2966.2005.09206.x)
- Booth, C. M., & Schaye, J. 2009, *MNRAS*, 398, 53, doi: [10.1111/j.1365-2966.2009.15043.x](https://doi.org/10.1111/j.1365-2966.2009.15043.x)
- Cappellari, M. 2017, *MNRAS*, 466, 798, doi: [10.1093/mnras/stw3020](https://doi.org/10.1093/mnras/stw3020)
- . 2022, arXiv e-prints, arXiv:2208.14974, <https://arxiv.org/abs/2208.14974>
- Cappellari, M., & Emsellem, E. 2004, *PASP*, 116, 138, doi: [10.1086/381875](https://doi.org/10.1086/381875)
- Carilli, C. L., & Taylor, G. B. 2000, *ApJL*, 532, L95, doi: [10.1086/312584](https://doi.org/10.1086/312584)
- Carnall, A. C. 2017, arXiv e-prints, arXiv:1705.05165, <https://arxiv.org/abs/1705.05165>
- Celotti, A., Padovani, P., & Ghisellini, G. 1997, *MNRAS*, 286, 415, doi: [10.1093/mnras/286.2.415](https://doi.org/10.1093/mnras/286.2.415)
- Costa, T., Sijacki, D., & Haehnelt, M. G. 2014, *MNRAS*, 444, 2355, doi: [10.1093/mnras/stu1632](https://doi.org/10.1093/mnras/stu1632)
- Curran, S. J. 2017, *A&A*, 606, A56, doi: [10.1051/0004-6361/201731666](https://doi.org/10.1051/0004-6361/201731666)
- . 2019, *MNRAS*, 484, 3911, doi: [10.1093/mnras/stz215](https://doi.org/10.1093/mnras/stz215)
- . 2021, *MNRAS*, 506, 1548, doi: [10.1093/mnras/stab1865](https://doi.org/10.1093/mnras/stab1865)
- Curran, S. J., Duchesne, S. W., Divoli, A., & Allison, J. R. 2016, *MNRAS*, 462, 4197, doi: [10.1093/mnras/stw1938](https://doi.org/10.1093/mnras/stw1938)
- Dey, A., Schlegel, D. J., Lang, D., et al. 2019, *AJ*, 157, 168, doi: [10.3847/1538-3881/ab089d](https://doi.org/10.3847/1538-3881/ab089d)
- Di Matteo, T., Springel, V., & Hernquist, L. 2005, *Nature*, 433, 604, doi: [10.1038/nature03335](https://doi.org/10.1038/nature03335)
- Fabian, A. C. 2012, *ARA&A*, 50, 455, doi: [10.1146/annurev-astro-081811-125521](https://doi.org/10.1146/annurev-astro-081811-125521)
- Gibson, R. R., Jiang, L., Brandt, W. N., et al. 2009, *ApJ*, 692, 758, doi: [10.1088/0004-637X/692/1/758](https://doi.org/10.1088/0004-637X/692/1/758)
- Guo, H., Shen, Y., & Wang, S. 2018, PyQSOFit: Python code to fit the spectrum of quasars, Astrophysics Source Code Library, record ascl:1809.008, <http://ascl.net/1809.008>
- Gupta, N., Jagannathan, P., Srianand, R., et al. 2021a, *ApJ*, 907, 11, doi: [10.3847/1538-4357/abcb85](https://doi.org/10.3847/1538-4357/abcb85)
- Gupta, N., Srianand, R., Shukla, G., et al. 2021b, *ApJS*, 255, 28, doi: [10.3847/1538-4365/ac03b5](https://doi.org/10.3847/1538-4365/ac03b5)
- Healey, S. E., Romani, R. W., Taylor, G. B., et al. 2007, *ApJS*, 171, 61, doi: [10.1086/513742](https://doi.org/10.1086/513742)
- Heckman, T. M. 2002, in *Astronomical Society of the Pacific Conference Series*, Vol. 254, Extragalactic Gas at Low Redshift, ed. J. S. Mulchaey & J. T. Stocke, 292, <https://arxiv.org/abs/astro-ph/0107438>
- Hopkins, P. F., & Elvis, M. 2010, *MNRAS*, 401, 7, doi: [10.1111/j.1365-2966.2009.15643.x](https://doi.org/10.1111/j.1365-2966.2009.15643.x)
- Hu, W., Wang, Y., Li, Y., et al. 2023, arXiv e-prints, arXiv:2305.02007, doi: [10.48550/arXiv.2305.02007](https://doi.org/10.48550/arXiv.2305.02007)
- Jiang, P., Yue, Y., Gan, H., et al. 2019, *Science China Physics, Mechanics, and Astronomy*, 62, 959502, doi: [10.1007/s11433-018-9376-1](https://doi.org/10.1007/s11433-018-9376-1)
- Jiang, P., Tang, N.-Y., Hou, L.-G., et al. 2020, *Research in Astronomy and Astrophysics*, 20, 064, doi: [10.1088/1674-4527/20/5/64](https://doi.org/10.1088/1674-4527/20/5/64)
- Kanekar, N., Prochaska, J. X., Ellison, S. L., & Chengalur, J. N. 2009, *MNRAS*, 396, 385, doi: [10.1111/j.1365-2966.2009.14661.x](https://doi.org/10.1111/j.1365-2966.2009.14661.x)
- Kanekar, N., Prochaska, J. X., Smette, A., et al. 2014, *MNRAS*, 438, 2131, doi: [10.1093/mnras/stt2338](https://doi.org/10.1093/mnras/stt2338)
- King, A. R. 2010, *MNRAS*, 402, 1516, doi: [10.1111/j.1365-2966.2009.16013.x](https://doi.org/10.1111/j.1365-2966.2009.16013.x)
- Lehnert, M. D., Tasse, C., Nesvadba, N. P. H., Best, P. N., & van Driel, W. 2011, *A&A*, 532, L3, doi: [10.1051/0004-6361/201117323](https://doi.org/10.1051/0004-6361/201117323)
- Li, D., Wang, P., Qian, L., et al. 2018, *IEEE Microwave Magazine*, 19, 112, doi: [10.1109/MMM.2018.2802178](https://doi.org/10.1109/MMM.2018.2802178)
- Maccagni, F. M., Morganti, R., Oosterloo, T. A., Geréb, K., & Maddox, N. 2017, *A&A*, 604, A43, doi: [10.1051/0004-6361/201730563](https://doi.org/10.1051/0004-6361/201730563)
- Maccagni, F. M., Morganti, R., Oosterloo, T. A., & Mahony, E. K. 2014, *A&A*, 571, A67, doi: [10.1051/0004-6361/201424334](https://doi.org/10.1051/0004-6361/201424334)
- Mahony, E. K., Morganti, R., Emonts, B. H. C., Oosterloo, T. A., & Tadhunter, C. 2013, *MNRAS*, 435, L58, doi: [10.1093/mnras/slt094](https://doi.org/10.1093/mnras/slt094)
- Mahony, E. K., Allison, J. R., Sadler, E. M., et al. 2022, *MNRAS*, 509, 1690, doi: [10.1093/mnras/stab3041](https://doi.org/10.1093/mnras/stab3041)
- McConnell, N. J., & Ma, C.-P. 2013, *ApJ*, 764, 184, doi: [10.1088/0004-637X/764/2/184](https://doi.org/10.1088/0004-637X/764/2/184)

- Morganti, R., Fogasy, J., Paragi, Z., Oosterloo, T., & Orienti, M. 2013, *Science*, 341, 1082, doi: [10.1126/science.1240436](https://doi.org/10.1126/science.1240436)
- Morganti, R., & Oosterloo, T. 2018, *A&A Rv*, 26, 4, doi: [10.1007/s00159-018-0109-x](https://doi.org/10.1007/s00159-018-0109-x)
- Morganti, R., Sadler, E. M., & Curran, S. 2015, in *Advancing Astrophysics with the Square Kilometre Array (AASKA14)*, 134, doi: [10.22323/1.215.0134](https://doi.org/10.22323/1.215.0134)
- Morganti, R., Tadhunter, C. N., & Oosterloo, T. A. 2005, *A&A*, 444, L9, doi: [10.1051/0004-6361:200500197](https://doi.org/10.1051/0004-6361:200500197)
- Murthy, S., Morganti, R., Oosterloo, T., & Maccagni, F. M. 2021, *A&A*, 654, A94, doi: [10.1051/0004-6361/202141566](https://doi.org/10.1051/0004-6361/202141566)
- Nan, R., Li, D., Jin, C., et al. 2011, *International Journal of Modern Physics D*, 20, 989, doi: [10.1142/S0218271811019335](https://doi.org/10.1142/S0218271811019335)
- Nan, R. D., Zhang, H. Y., Zhang, Y., et al. 2016, *Acta Astronomica Sinica*, 57, 623
- Petrov, L. 2021, *AJ*, 161, 14, doi: [10.3847/1538-3881/abc4e1](https://doi.org/10.3847/1538-3881/abc4e1)
- Sadler, E. M., Moss, V. A., Allison, J. R., et al. 2020, *MNRAS*, 499, 4293, doi: [10.1093/mnras/staa2390](https://doi.org/10.1093/mnras/staa2390)
- Schinzel, F. K., Petrov, L., Taylor, G. B., & Edwards, P. G. 2017, *ApJ*, 838, 139, doi: [10.3847/1538-4357/aa6439](https://doi.org/10.3847/1538-4357/aa6439)
- Souchay, J., Andrei, A. H., Barache, C., et al. 2012, *A&A*, 537, A99, doi: [10.1051/0004-6361/201117954](https://doi.org/10.1051/0004-6361/201117954)
- Struve, C., Oosterloo, T., Sancisi, R., Morganti, R., & Emonts, B. H. C. 2010, *A&A*, 523, A75, doi: [10.1051/0004-6361/201015311](https://doi.org/10.1051/0004-6361/201015311)
- Su, R., Sadler, E. M., Allison, J. R., et al. 2022, *MNRAS*, 516, 2947, doi: [10.1093/mnras/stac2257](https://doi.org/10.1093/mnras/stac2257)
- Su, R., Mahony, E. K., Gu, M., et al. 2023, *MNRAS*, doi: [10.1093/mnras/stad370](https://doi.org/10.1093/mnras/stad370)
- Sullivan, M., Mobasher, B., Chan, B., et al. 2001, *ApJ*, 558, 72, doi: [10.1086/322451](https://doi.org/10.1086/322451)
- Varenius, E., Conway, J. E., Batejat, F., et al. 2019, *A&A*, 623, A173, doi: [10.1051/0004-6361/201730631](https://doi.org/10.1051/0004-6361/201730631)
- Veilleux, S., Cecil, G., & Bland-Hawthorn, J. 2005, *ARA&A*, 43, 769, doi: [10.1146/annurev.astro.43.072103.150610](https://doi.org/10.1146/annurev.astro.43.072103.150610)
- Veilleux, S., Maiolino, R., Bolatto, A. D., & Aalto, S. 2020, *A&A Rv*, 28, 2, doi: [10.1007/s00159-019-0121-9](https://doi.org/10.1007/s00159-019-0121-9)
- Wagner, A. Y., & Bicknell, G. V. 2011, *ApJ*, 728, 29, doi: [10.1088/0004-637X/728/1/29](https://doi.org/10.1088/0004-637X/728/1/29)
- Wagner, A. Y., Bicknell, G. V., & Umemura, M. 2012, *ApJ*, 757, 136, doi: [10.1088/0004-637X/757/2/136](https://doi.org/10.1088/0004-637X/757/2/136)
- Weymann, R. J., Morris, S. L., Foltz, C. B., & Hewett, P. C. 1991, *ApJ*, 373, 23, doi: [10.1086/170020](https://doi.org/10.1086/170020)
- Xu, Y.-D., Cao, X., & Wu, Q. 2009, *ApJL*, 694, L107, doi: [10.1088/0004-637X/694/2/L107](https://doi.org/10.1088/0004-637X/694/2/L107)
- Zhang, B., Zhu, M., Wu, Z.-Z., et al. 2021, *MNRAS*, 503, 5385, doi: [10.1093/mnras/stab754](https://doi.org/10.1093/mnras/stab754)
- Zheng, Z., Li, D., Sadler, E. M., Allison, J. R., & Tang, N. 2020, *MNRAS*, 499, 3085, doi: [10.1093/mnras/staa3033](https://doi.org/10.1093/mnras/staa3033)
- Zhuang, M.-Y., & Ho, L. C. 2019, *ApJ*, 882, 89, doi: [10.3847/1538-4357/ab340d](https://doi.org/10.3847/1538-4357/ab340d)
- Zubovas, K., & King, A. 2012, *ApJL*, 745, L34, doi: [10.1088/2041-8205/745/2/L34](https://doi.org/10.1088/2041-8205/745/2/L34)